Sensors and Actuators B 229 (2016) 200–208

Contents lists available at ScienceDirect

Sensors and Actuators B: Chemical

journal homepage: www.elsevier.com/locate/snb

High performance mixed potential type acetone sensor based on stabilized zirconia and $NiNb_2O_6$ sensing electrode

Fangmeng Liu, Xue Yang, Bin Wang, Yehui Guan, Xishuang Liang*, Peng Sun, Geyu Lu*

State Key Laboratory on Integrated Optoelectronics, College of Electronic Science and Engineering, Jilin University, 2699 Qianjin Street, Changchun 130012, China

ARTICLE INFO

Article history:
Received 18 November 2015
Received in revised form
21 December 2015
Accepted 26 January 2016
Available online 4 February 2016

Keywords:
$NiNb_2O_6$
Acetone sensor
YSZ
Mixed potential

ABSTRACT

A high performance mixed potential type gas sensor based on stabilized zirconia (YSZ) and $NiNb_2O_6$ as sensing electrode was fabricated and used for detection of acetone at 650 °C. $NiNb_2O_6$ prepared via a facile sol–gel method and sintered at different temperatures was characterized using X-ray diffraction (XRD) and field-emission scanning electron microscopy (FESEM). The present study mainly focused on the effect of sintering temperature (800 °C, 1000 °C, 1200 °C) of $NiNb_2O_6$-SE materials on acetone sensing characteristics at 650 °C. Results indicated that the sensor using $NiNb_2O_6$-SE sintered at 1000 °C exhibited the largest sensitivity to acetone in the concentration range of 5–500 ppm at 650 °C, which the slope was −79 mV/decade. The response for the sensor attached with a $NiNb_2O_6$-SE sintered at 1000 °C to 100 ppm of acetone was approximately −113 mV. Moreover, the present sensor could detect even 500 ppb acetone with an acceptable response. The present device also displayed fast response and recovery times, good repeatability, slight sensitive effect to humidity, small drifts in 40 days measured periods, and acceptable selectivity at 650 °C. Additionally, the mixed potential mechanism was further demonstrated by polarization curve.

1. Introduction

The universal environmental pollution problems have arisen frequently in some cities in China, represented by simultaneous high levels of ground-level ozone and PM2.5. Volatile organic compounds (VOC) defined as a group of carbon-containing compounds that evaporate readily at room temperature are important precursors leading to the formation of ozone and fine particles [1,2]. Acetone as a species of VOC is emitted into the atmosphere from both natural and anthropogenic sources, such as biogenic emission, vehicular exhaust, solvent utilization, and industrial emission, etc. [3–5]. This hazardous air pollutant has been associated with serious adverse health effects, including respiratory and neurological illnesses when long-term inhalation or contact. To properly address the related air quality and health effect problem, reliable detection of acetone is critical for developing effective control technologies and coping strategies. Several acetone detection methods, such as gas chromatography/mass spectroscopy (GC/MS) and differential mobility spectroscopy (DMS) have been proposed for the accurate analysis [6,7]. In general, however, these types of methods do not meet the requirements of portability, cost-effective performance, real-time diagnosis and so forth. In this regard, the gas sensors offering high sensitivity, low limit of detection, good stability are receiving increased attention due to the great potential for realization of low fabrication costs, real-time detections and miniaturization of portable devices.

Among the various VOC sensors reported [8–16], mixed potential type gas sensors utilizing yttria-stabilized zirconia (YSZ) as solid electrolyte have been designed and investigated in a wide area of application. For mixed potential gas sensor, the category of sensing electrode material is vital to the improved sensing performance of the sensor. However, the development of sensing electrode material for YSZ-based mixed potential type acetone sensor is rarely reported. Among them, Kasalizadeh et al. reported Yttria-stabilized zirconia (YSZ)-based sensors using coupled metal oxide-doped Pt/SnO_2 sensing electrodes, result in the good response and lower response and recovery times [17]. Our group fabricated the mixed-potential-type acetone sensors using YSZ as solid electrolyte and $Zn_3V_2O_8$ composite oxide as sensing electrode, which exhibit a low detection limit of 1 ppm, and effective sensing characteristics to acetone [18]. Although above-mentioned YSZ-based electrochemical sensors displayed good performance in some respects, from the perspective of practical application, the design and development of the sensor with excellent sensitivity, long-term stability, especially

* Corresponding authors. Fax: +86 431 85167808.
E-mail addresses: liangxs@jlu.edu.cn (X. Liang), lugy@jlu.edu.cn (G. Lu).

http://dx.doi.org/10.1016/j.snb.2016.01.128
0925-4005/

moisture resistance and the lowest detection limit to acetone is still to be desperately needed.

Herein, for the first time, a novel type $NiNb_2O_6$ composite oxide is synthesized with a facile sol–gel method and used as sensing electrode for fabricating YSZ-based mixed-potential-type acetone sensor. The effect of different sintering temperatures of $NiNb_2O_6$-SE on sensing characteristics is studied. The results turn out that the sensor attached with $NiNb_2O_6$-SE sintered at 1000 °C displays the largest sensitivity to acetone in the examined range of 5–500 ppm at 650 °C. Additionally, the gas sensing properties of the present device to acetone are systematically investigated and the sensing mechanism is discussed.

2. Experimental

2.1. Preparation and characterization of $NiNb_2O_6$ sensing electrode material

The $NiNb_2O_6$ was synthesized via a sol–gel method from Nickel nitrate hexahydrate ($Ni(NO_3)_2{\cdot}6H_2O$), Niobium oxide (Nb_2O_5), HF acid (40%), Ammonium hydroxide ($NH_3{\cdot}H_2O$), Citric acid (CA), and Ammonium nitrate (NH_4NO_3). All of reagents were of analytical grade without further purification. In a typical synthesis process, 3 mmol Nb_2O_5 was dissolved in a certain amount of HF acid after heating in water bath of 80 °C. Then, ammonia hydroxide solution was dropwise added to the above solution until the PH value was up to 9 to obtain $Nb_2O_5{\cdot}nH_2O$ precipitate under stirring constantly. The precipitate was filtered, washed, and dissolved in citric acid aqueous solution and stirred at 80 °C for 2 h. Then, the stoichiometric $Ni(NO_3)_2{\cdot}6H_2O$ and NH_4NO_3 (the molar ratio of $Ni/Nb/NH_4NO_3$ = 1:2:12) were added into the solution described above and then stirred at 80 °C until to a gel was obtained. The resultant gel was maintained at 80 °C for 24 h at vacuum drying oven. The precursor gel was then introduced into a muffle furnace and sintered at 800, 1000, and 1200 °C for 2 h to get target products, respectively.

The structural properties of the products were characterized with Rigaku wide-angle X-ray diffractometer (D/max rA, using Cu Kα radiation at wave length = 0.1541 nm) in the angular range of 20–80°. Field-emission scanning electron microscopy (FESEM) measurements of surface morphology of the $NiNb_2O_6$-SE materials were performed using a JEOL JSM-7500F microscope with an accelerating voltage of 10 kV.

2.2. Fabrication and measurement of gas sensor

The sensor was fabricated using the YSZ plate (8 mol% Y_2O_3-doped, 2 mm × 2 mm square, 0.2 mm thickness, provided by Tosoh Corp., Japan). A point-shaped and a narrow stripe-shaped Pt electrode (reference electrode, RE) were formed on two ends of the YSZ plate using a commercial Pt paste (Sino-platinum Metals Co., Ltd.), and sintered at 1000 °C. The various sensing materials obtained by sintering at different temperature (800, 1000 and 1200 °C) were mixed with a minimum quantity of deionized water, respectively. Then, the resultant paste was applied on the point-shaped Pt to form stripe-shaped sensing electrode (SE), and then the device was sintered at 800 °C for 2 h to gain good contact between the sensing electrode and electrolyte. The Pt heater printed on Al_2O_3 substrate was then fixed to the YSZ plate by the inorganic adhesive, which provided the required heating temperature for the sensor. The schematic of the fabricated sensor is shown in Fig. 1.

The gas sensing characteristics of the fabricated sensors were measured by a conventional static method. The detailed gas sensing measurement technique as followed: the sensor fabricated was placed in airtight chamber with volume of 1 L. Before the measurement, the pure air was filled using an air pump. Then, a certain amount of acetone or other solvents were injected into the chamber via a special airlock at side of the chamber using a microsyringe and the ventilators in the chamber were working fast to make the test gases distributed uniformly in the chamber. The whole process was controlled by intelligent system and the time it took was less than a second [19,20]. The electric potential difference (V) between the SE and the RE was measured with a digital electrometer (Rigol Technologies, Inc., DM3054, China) when the sensor was exposed to air or sample gas. The results obtained were recorded with a computer connected to the electrometer. The desired concentration of sample gas was obtained by the static liquid gas distribution method, which was calculated by the following formula [21,22].

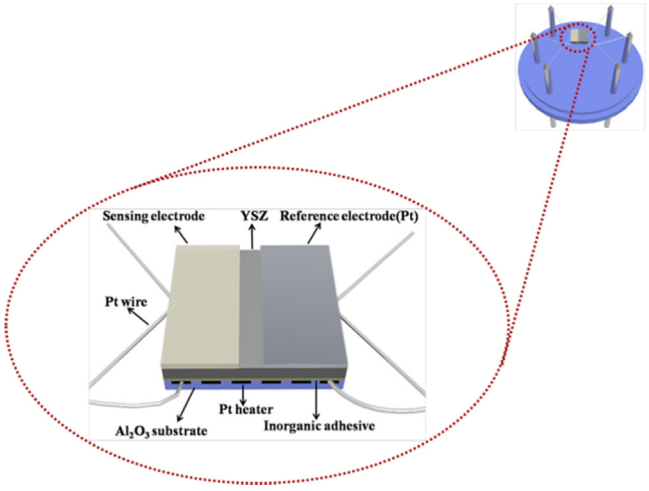

Fig. 1. Schematic diagram of fabricated sensor.

$$C = \frac{22.4 \times \rho \times \varphi \times V_1}{M \times V_2} \times 1000$$

where C(ppm) is the desired target gas concentration; ρ(g/mL) the density of the liquid; φ the required gas volume fraction; V_1 (μL) and V_2 (L) the volume of the liquid and chamber, respectively; and M (g/mol) the molecular weight of the liquid. The current–voltage (polarization) curves of the sensor were carried out via the potentiodynamic method (CHI650C, Instrument corporation of Shanghai, China) using a two-electrode configuration in the base gas (air) and the different concentrations of acetone gas (50, 100, 200, and 300 ppm) at 650 °C.

3. Results and discussion

X-ray diffraction (XRD) was used to identify the crystallographic structure and crystallinity of the as-synthesized products. Fig. 2 shows the XRD pattern of $NiNb_2O_6$ composite oxide annealed at different temperatures. The sharp diffraction features suggest the good crystalline nature of the prepared $NiNb_2O_6$ composite oxide sensing electrode materials. The diffraction peaks of $NiNb_2O_6$ sintered at 800, 1000 and 1200 °C are readily indexed to orthorhombic structure of $NiNb_2O_6$ oxide standard XRD patterns, which agreed well with the reported values from the Joint Committee on Powder Diffraction Standards card (JCPDS#32–694). The morphologies of $NiNb_2O_6$-SE sintered at different temperatures (800, 1000, and 1200 °C) were studied by FESEM, as shown in Fig. 3. It can be observed that the pore and particle size increased gradually with the increasing of sintering temperature. Such porous structure contributed to diffusion of the gas molecular within the material.

In order to study the effect of sintering temperature on the sensing performances, the sensors using $NiNb_2O_6$-SE calcinated

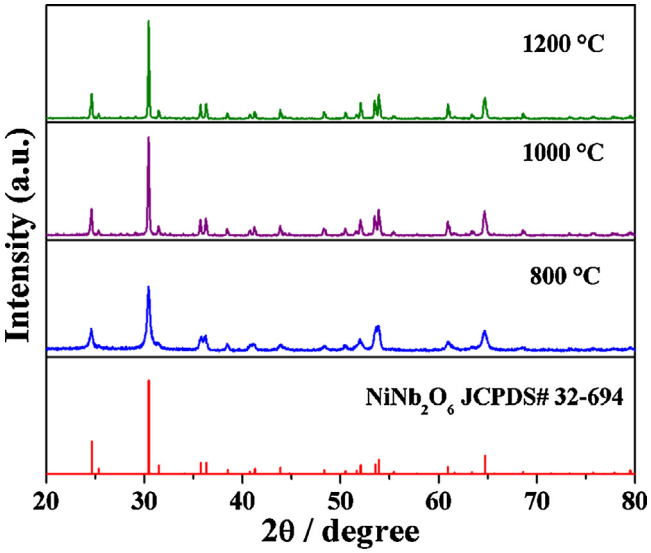

Fig. 2. XRD pattern of $NiNb_2O_6$ composite oxide material sintered at 800, 1000 and 1200 °C.

at 800 °C, 1000 °C and 1200 °C were fabricated and the dependence of ΔV on the logarithm of acetone concentrations for these sensor were measured and shown in Fig. 4. It is apparent that the electric potential difference (ΔV) of three sensors fabricated varied almost linearly with the logarithm of acetone concentrations in the examined range of 5–500 ppm at 650 °C, which is typical for the mixed-potential type sensor [23–25]. Also, the sensor utilizing $NiNb_2O_6$-SE annealed at 1000 °C exhibited the almost largest response values to each concentrations of acetone in the range of examined range and the highest sensitivity (slope) comparing with the devices attached with $NiNb_2O_6$-SE sintered at other temperatures. The reason for this result may be partially explained from the following aspects. The sensing characteristics of the present devices abide by the mixed-potential theory, which has been demonstrated by Miura and co-workers [24,26,27]. Based on this, the sensor can be presented as the following electrochemical cells:

In air: O_2, $NiNb_2O_6$/YSZ/Pt, O_2

In sample gas: $C_3H_6O + O_2$, $NiNb_2O_6$/YSZ/Pt, $C_3H_6O + O_2$

Under the acetone gas atmosphere, the electrochemical reactions of cathodic (1) and anodic (2) (the cathodic reaction of O_2 and the anodic reaction of acetone) take place simultaneously at the TPB (triple phase boundary, the interface of $NiNb_2O_6$-SE, acetone and YSZ) and form a local cell. When the rates of two electrochemical reactions are equal to each other, the dynamic equilibrium is reached, and the electrode potential is called the mixed potential. The potential difference of the sensing electrode and reference electrode is obtained as the sensing signal.

$$\text{Cathodicreaction}: O_2 + 4e^- \rightarrow 2O^{2-} \quad (1)$$

$$\text{Anodicreaction}: 1/4C_3H_6O + 2O^{2-} \rightarrow 3/4CO_2 + 3/4H_2O + 4e^- \quad (2)$$

In regard to the present device, the sensing signal is strongly dependent on the acetone concentration passed through SE layer and reached to TPB of $NiNb_2O_6$/YSZ/Acetone and degree of electrochemical reactions at TPB. Taking consideration of these aspects, the more gas channel in SE layer and higher electrochemical reaction action to acetone induced higher sensing performance. As indicated in Fig. 3, the sizes of pore and particle for $NiNb_2O_6$-SE increased with the increasing of the sintering temperatures. The larger porous channels decreased the consumption of acetone in the process of diffusion in $NiNb_2O_6$ electrode layer and facilitate

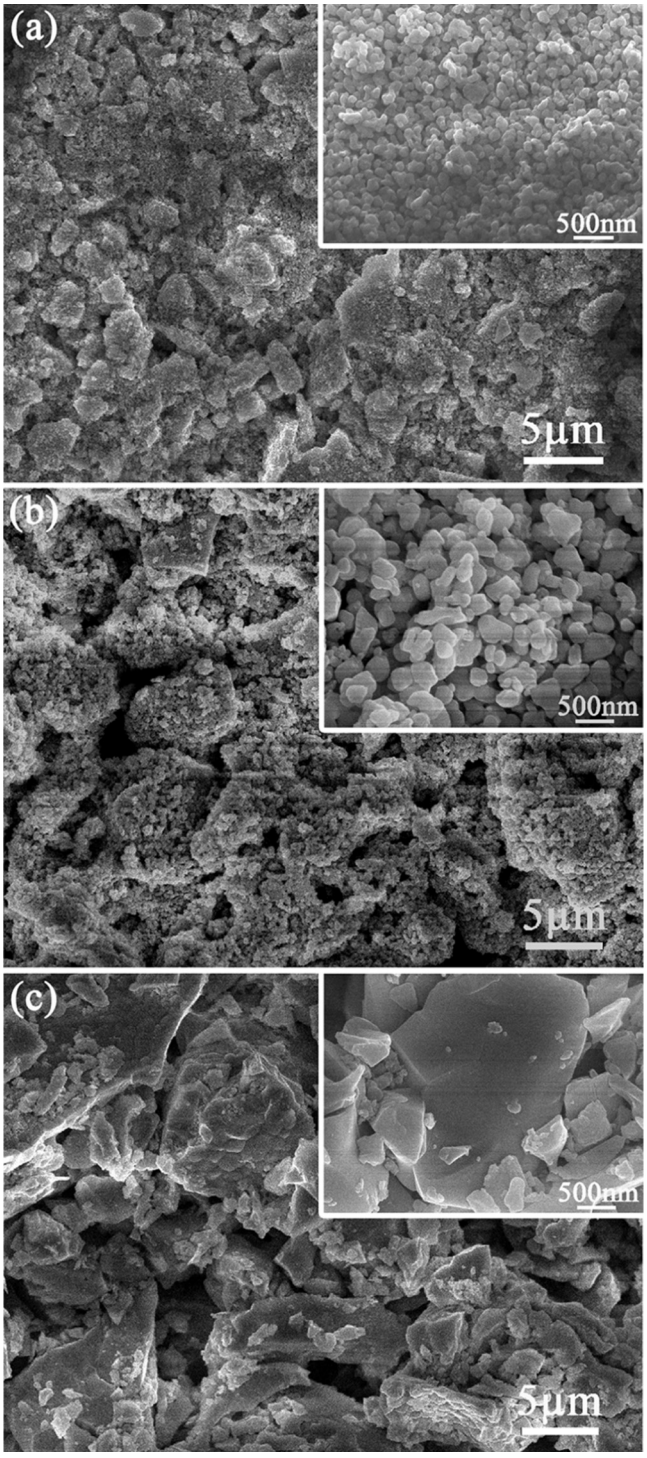

Fig. 3. SEM images of $NiNb_2O_6$-SEs sintered at different temperatures (a) 800 °C; (b) 1000 °C (c) 1200 °C.

more acetone gas to reach the TPB, which participated directly in electrochemical reactions. In this way, the sensitivity of sensor may be improved with the increasing of sintering temperature. However, the particles of $NiNb_2O_6$ became too large with the further increase of annealing temperature and then the interface area of the enlarged particle and YSZ increased, but TPB area reduced as shown in Fig. 5. In this case, the electrochemical reaction active sites decreased because of reduction of TPB length, that is, the sensitivity of the sensor attached with $NiNb_2O_6$-SE sintered at

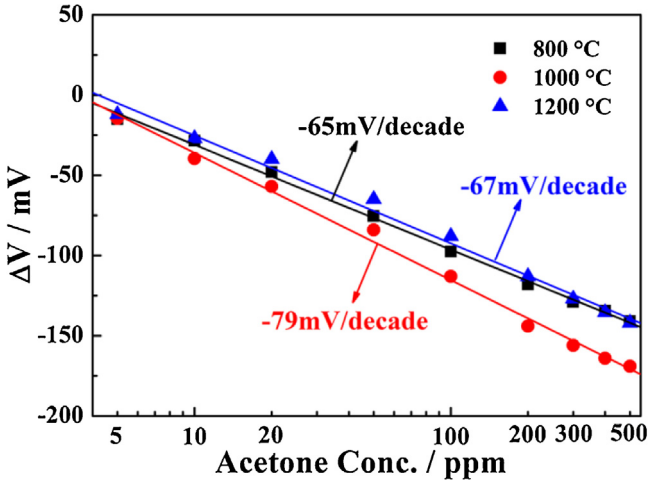

Fig. 4. Dependence of ΔV on the logarithm of acetone concentrations for the sensors using $NiNb_2O_6$-SEs calcined at 800 °C, 1000 °C, and 1200 °C in the range of 5–500 ppm at 650 °C.

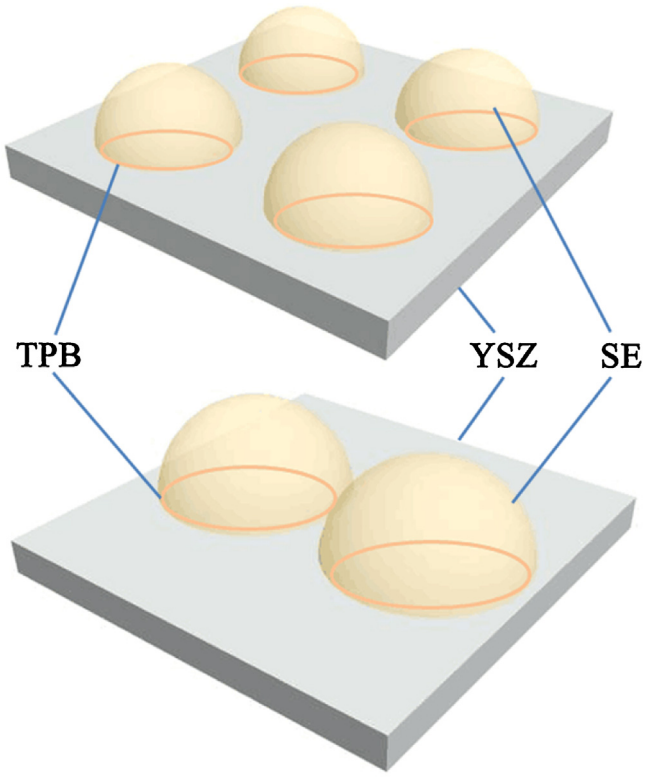

Fig. 5. Schematic view of different particle sizes of sensing electrode and YSZ.

1200 °C to acetone decreased obviously, compared with those of sintered at 800 and 1000 °C. Based on considering these factors, the excellent balance of the diffusion of acetone passed through $NiNb_2O_6$-SE layer and TPB area was formed when the annealed temperature is 1000 °C. Additionally, the $NiNb_2O_6$ oxide material showed the prominent catalytic property [28,29]. It was beneficial to accelerate the electrochemical reaction and resulted in high sensitivity. Therefore, the sensor using $NiNb_2O_6$ sintered at 1000 °C exhibited the largest sensitivity and then was paid considerable attentions to investigate in the following sections. In order to further illuminate the reason for the highest sensitivity of the sensor utilizing $NiNb_2O_6$-SE annealed at 1000 °C and validate the proposed mixed-potential mechanism, the polarization curves of the sensor attached with $NiNb_2O_6$-SE sintered at different temperatures in air and 100 ppm acetone and the polarization curves of the sensor utilizing $NiNb_2O_6$-SE sintered at 1000 °C in different concentrations of acetone at 650 °C were measured and shown in Fig. 6**(a) and (b)** [30]. The cathodic polarization curve was obtained in air, and the anodic polarization curve was obtained by subtracting in air from in sample gas (different concentration of acetone + air). It is clearly seen that the polarization curve for the anodic reaction of acetone for the device using $NiNb_2O_6$-SE sintered at 1000 °C shifts downward to higher current values, compared with others of that 800 °C and 1200 °C. This indicates that sensor attached with $NiNb_2O_6$-SE sintered at 1000 °C exhibits the highest electrochemical catalytic activity to anodic reaction (2). In this case, the sensor attached with $NiNb_2O_6$-SE annealed at 1000 °C displayed the highest sensitivity to acetone at 650 °C. Additionally, the mixed potential can be estimated from the intersection of the cathodic and anodic polarization curves [31,32]. Based on the comparison of the mixed potential estimated values and the potential difference values experimentally observed for fabricated three devices and the sensor utilizing $NiNb_2O_6$-SE annealed at 1000 °C to different concentration of acetone at 650 °C, in Table 1. The estimated values are in close proximity to those observed values under all circumstances. These coincidences further indicate that the present sensors supported the sensing mechanism involving the mixed potential [27,30,33,34].

The mixed potentials of the sensor fabricated can be treated quantitatively, as has been done before [23,35]. The cathodic and

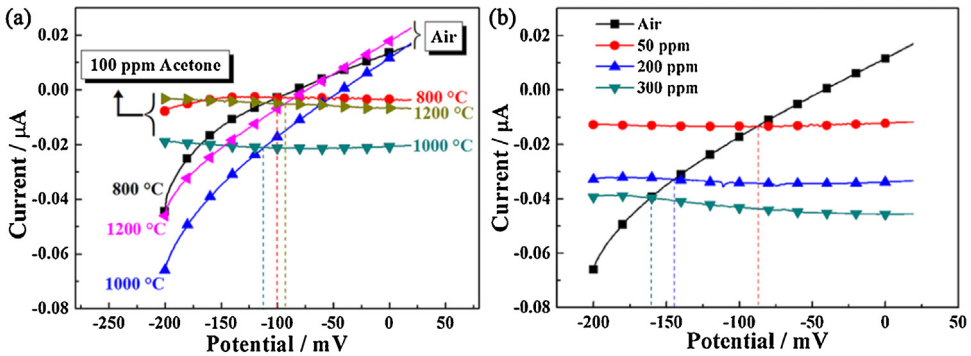

Fig. 6. (a) Polarization curves in air and 100 ppm acetone at 650 °C for the sensor using $NiNb_2O_6$-SE sintered at 800 °C, 1000 °C and 1200 °C (b) polarization curves in different concentrations of acetone for the sensor attached with $NiNb_2O_6$-SE sintered at 1000 °C.

Table 1
Comparison of the mixed potential estimated and the potential difference value observed for the sensors attached with $NiNb_2O_6$-SEs sintered at 800 °C, 1000 °C, and 1200 °C.

Sensors	Acetone Conc. (ppm)	Mixed potential (estimated) (mV)	Potential difference value (observed) (mV)
$NiNb_2O_6$ (800 °C)-SE	100	−100	−97.5
$NiNb_2O_6$ (1000 °C)-SE	100	−112	−113
$NiNb_2O_6$ (1200 °C)-SE	100	−92.5	−89
$NiNb_2O_6$ (1000 °C)-SE	50	−87	−84
$NiNb_2O_6$ (1000 °C)-SE	200	−144.5	−144
$NiNb_2O_6$ (1000 °C)-SE	300	−160	−156

anodic current densities for reactions (1) and (2) can be expressed by the following equations, respectively.

$$i_{O_2} = i^0_{O_2} \exp\left[-\frac{4\alpha F\left(V - V^0_{O_2}\right)}{RT}\right] \quad (3)$$

$$i_{\text{Acetone}} = i^0_{\text{Acetone}} \exp\left[\frac{4\beta F\left(V - V^0_{\text{Acetone}}\right)}{RT}\right] \quad (4)$$

here V is the electrode potential; F is the Faraday constant; V^0 and i^0 are the electrode potential and the exchange current density at equilibrium; α and β represent transfer coefficient; R is the gas constant and T is the temperature. We assume that i^0 obey the following kinetic equations.

$$i^0_{O_2} = -B_1 C^m_{O_2} \quad (5)$$

$$i^0_{\text{Acetone}} = B_2 C^n_{\text{Acetone}} \quad (6)$$

where B_1, B_2, m, and n are constants, C_{O_2} and C_{Acetone} represent the concentration of O_2 and Acetone, respectively, and i^0_{Acetone} and $i^0_{O_2}$ are values with opposite signs. When the cathodic and anodic electrochemical reactions reach equilibrium, $i_{\text{Acetone}} + {}^{i}O_2 = 0$ is established, and the mixed potential (V_M) is defined as the electrode potential (ΔV) and represented by following equation:

$$V_M = V_0 + mA \ln C_{O_2} - nA \ln C_{\text{Acetone}} \quad (7)$$

here V_0 and A are given in Eqs. (8) and (9), respectively.

$$V_0 = \frac{RT}{(4\alpha + 4\beta)F} \ln \frac{B_1}{B_2} + \frac{2\alpha V^0_{O_2} + 2\beta V^0_{\text{Acetone}}}{2\alpha + 2\beta} \quad (8)$$

$$A = \frac{RT}{(4\alpha + 4\beta)F} \quad (9)$$

in the case of fixed concentration of O_2, Eq. (7) is simplified to the following equation.

$$V_M = V_0 - nA \ln C_{\text{Acetone}} \quad (10)$$

It can be clearly seen that, from Eq. (10), V_m varies decrease linearly with an increase in the logarithm of acetone concentration under the fixed concentration value of O_2, which has been observed experimentally in Fig. 4 very well. Such theoretical analysis further demonstrated that the present sensor obeyed the mixed potential mechanism.

It is well known that the response of the sensor depended strongly on the operation temperature. Therefore, the optimal operating temperature of the sensor attached with $NiNb_2O_6$-SE annealed at 1000 °C to acetone was investigated. The response and recovery transients for the sensor using $NiNb_2O_6$-SE sintered at 1000 °C to 100 ppm acetone at different operating temperatures are shown in Fig. 7. It can be observed that the response to 100 ppm acetone for fabricated sensor tended to increase initially with the increasing of the operating temperature and the highest response value was obtained at 650 °C. Above 650 °C, however, the response of the sensor tended to decrease. The occurrence of the electrochemical reaction for the present device at TPB needed definite

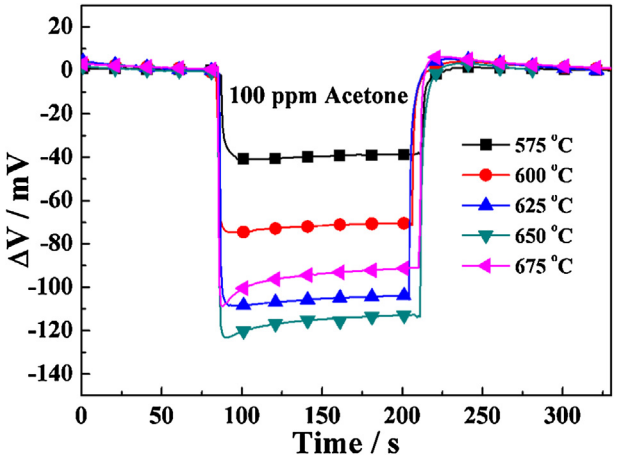

Fig. 7. Response and recovery transients for the sensor using $NiNb_2O_6$-SE sintered at 1000 °C to 100 ppm acetone at different operating temperatures.

activation energy [36]. The electrochemical reaction did not gain enough activation energy at below 650 °C, thus, the sensitivity of the sensor to acetone increased with the increasing of temperature. However, the desorption process of acetone exhibited dominant at above 650 °C, and the amount of acetone adsorbed on $NiNb_2O_6$ became less and less along with the increasing of temperature. Hence, the response of the sensor to acetone decreased with further increases in operating temperature. Consequently, the optimal operating temperature for the present sensor was considered to be 650 °C.

The response transients of fabricated sensor attached with $NiNb_2O_6$-SE annealed at 1000 °C toward different concentrations of acetone in the range of 5–500 ppm was examined at 650 °C and the results obtained are shown in Fig. 8. It is obvious that the present device exhibits fast response and recovery rates in the range of measured concentrations and the typical 90% response and recovery times toward different concentrations of acetone are all less than 10s. As indicated in Fig. 3**(b)**, the more and larger porous channels of sensing electrode layer facilitated acetone gas to reach the TPB and participated directly in electrochemical reactions, which shortened the time in the diffusion process. Moreover, according to the measurement results of polarization curves and complex impedance, the catalytic activity to electrochemical reaction of acetone for the sensor present fabricated was high, which accelerated the reaction rate. Based on these factors, the present sensor displayed rapid response-recovery times. The response for the sensor attached with $NiNb_2O_6$-SE annealed at 1000 °C to 100 ppm acetone at 650 °C was −113 mV. It also can be seen that, from inset of Fig. 8**(a)**, the present sensor even could detect 500 ppb acetone, which the response value is −1.2 mV. Furthermore, the dependence of ΔV for the sensor attached with $NiNb_2O_6$-SE annealed at 1000 °C on the acetone concentration in the examined range at 650 °C is shown in Fig. 8**(b)**. In this case, almost linear relationships between the ΔV and the logarithm of acetone concentration in the both range of 0.5–5 ppm and 5–500 ppm at 650 °C were observed, which conforms to mixed potential type model. The ΔV of the

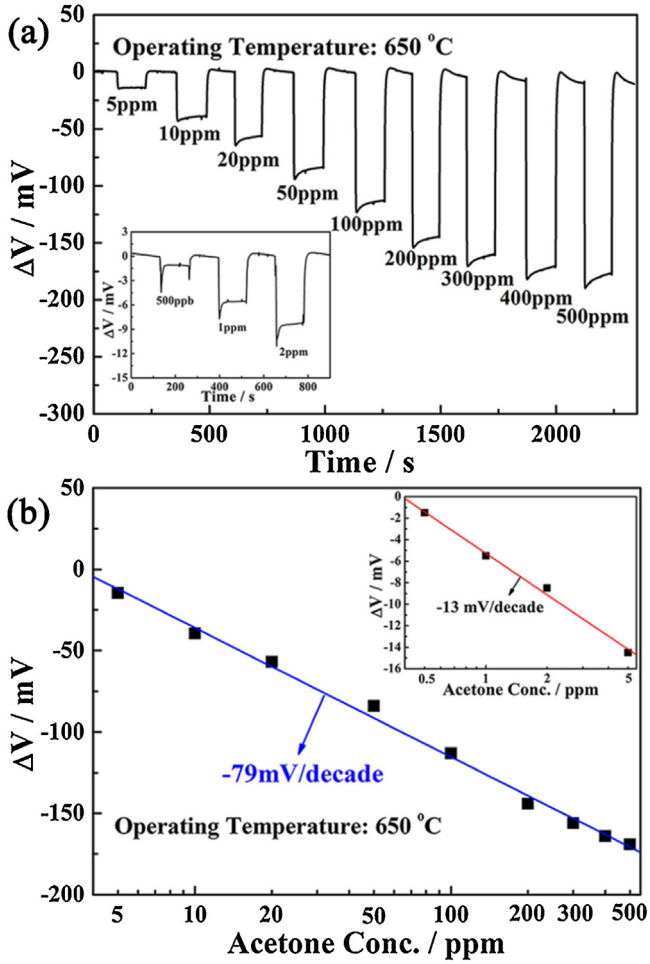

Fig. 8. (a) Response transient curves for the sensor attached with $NiNb_2O_6$-SE sintered at 1000 °C toward different concentrations of acetone in the range of 5–500 ppm at 650 °C. (b) Dependence of ΔV for the sensor attached with $NiNb_2O_6$-SE sintered at 1000 °C on the acetone concentration at 650 °C.

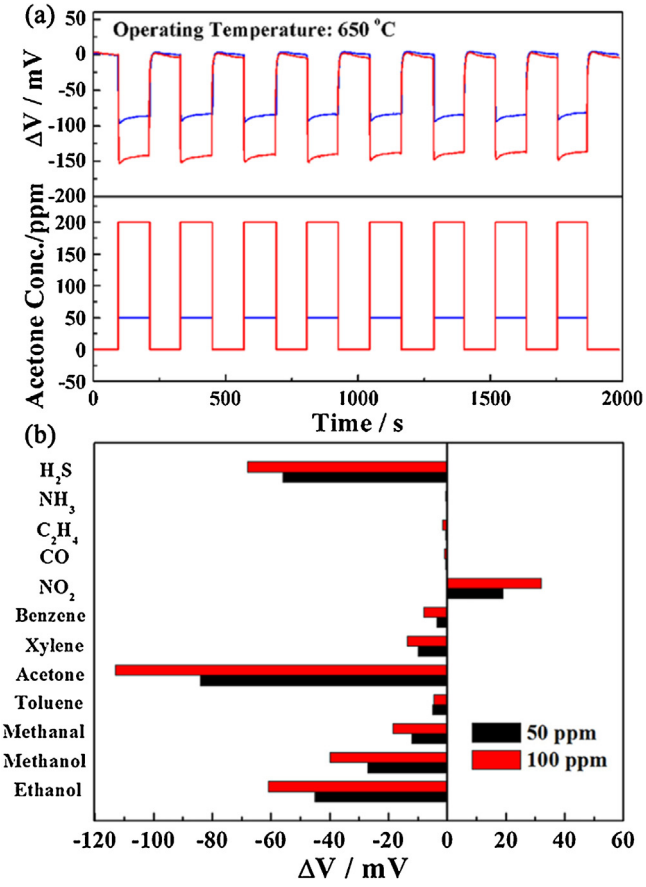

Fig. 9. (a) Continuous response-recovery transients to 50 ppm and 200 ppm acetone for the sensor attached with $NiNb_2O_6$-SE sintered at 1000 °C at 650 °C; (b) cross-sensitivities for the sensor attached with $NiNb_2O_6$-SE sintered at 1000 °C to various gases at 650 °C.

device exhibited segmentally linear relationship to the logarithm of acetone concentration and the slope was −13 mV/decade in the range of 0.5–5 ppm and −79 mV/decade in the range of 5–500 ppm, respectively. The reason for the occurrence of such a linear dependence of acetone sensitivity is may be followed. As known very well, the electrochemical reaction for the present mixed potential type acetone sensor occurred at the TPB. And the sensing signal of the sensor depended on the concentration of acetone at TPB of $NiNb_2O_6$-SE and the amount of active sites of TPB. For the low concentration range of acetone (0.5–5 ppm), the amount of TPB active sites for the present sensor are enough to provide the electrochemical reaction, thereby, the sensitivity of the sensor are mainly related to the amount of acetone, which reached the TPB of $NiNb_2O_6$-SE and directly participated in the electrochemical reaction. When the sensor is exposed to the acetone atmosphere, the acetone gas need pass through the sensing electrode layer and reach the TPB, which participate in the electrochemical reaction. Although with porous channels in sensing electrode layer, a certain amount of gas was still consumed in the process of diffusion. When the concentration of the measured acetone is at a lower level (0.5–5 ppm), the acetone consumption in the process of diffusion accounted for the proportion of the total quantity of acetone is larger than that of higher acetone concentration (5–500 ppm). Therefore, the relatively low sensitivity to acetone concentration in the range of 0.5–5 ppm was observed. Moreover, the continuous response-recovery and selectivity for gas sensor is important sensing performance parameters.

The continuous response-recovery transients of the present sensor to 50 and 200 ppm acetone at 650 °C, as illustrated in Fig. 9**(a)**. It is clearly seen that the responses of the present device to 50 and 200 ppm acetone have little fluctuation and the best change error of continuous responses were 2.4% and −7.6% in the examined eight-time cycles, which indicated that the sensor exhibited good repeatability. Fig. 9**(b)** shows the cross- sensitivities for the sensor attached with $NiNb_2O_6$-SE annealed at 1000 °C to various gases at 650 °C, such as toluene, benzene, NO_2 and NH_3, etc. It is obvious that the sensor present fabricated exhibited relative high responses to 50 and 100 ppm of acetone comparing with those of other interfering gases. But, the effect of the ethanol and H_2S as coexistence gas on acetone response for the fabricated sensor could not be ignored. Thus, the present device is insufficient in selectivity. The improvement of selectivity to ethanol and H_2S remains to be further investigated in the future work. On the whole, however, the present sensor still displayed acceptable selectivity to most of various interfering gases. Additionally, in order to explain clearly the mechanism of selectivity to acetone, the complex impedance of the sensor fabricated in 100 ppm of various test gases including acetone, ethanol, methanol and methanal is investigated and results obtained are shown in Fig. 10. Based on reported previously [37–39], the total resistance of the sensor seems to be affected by the interfacial resistance between the SE and YSZ. The interfacial resistance is given by the resistance value at the intersection of the large semi-arc with the real axis at lower frequencies (around 0.1 Hz). Evidently, when the sensor was exposed to 100 ppm of acetone, the interfacial resistance at the lower frequency range was obviously decreased compared with the interfacial resistance measured in other gases.

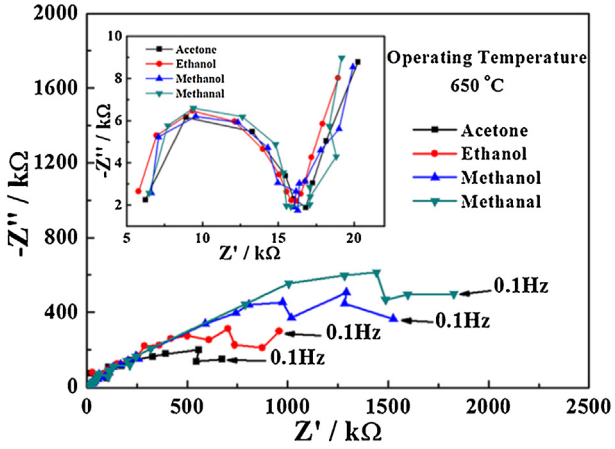

Fig. 10. Complex impedance curves in 100 ppm of various tested gases for the sensor attached with $NiNb_2O_6$-SE sintered at 1000 °C at 650 °C.

Changes in the interface resistance measured in different atmosphere revealed the electrochemical catalytic activity toward the examined gas species [40], thus, it can be speculated that the catalytic activity to the electrochemical reaction of acetone for present sensor was high. As a result, the higher electrochemical catalytic reaction activities generated highest sensing magnitude toward acetone.

For a point of view in actual application of the sensor, the sensitivity to a target gas should not be affected by the change in a surrounding condition. The water-vapor resistance and stability of sensor are two vital factors for evaluating sensing performance, thus, the responses for the sensor attached with $NiNb_2O_6$-SE sintered at 1000 °C to 100 ppm acetone in the relative humidity (RH) range of 20–98% and the long-term stability of the present sensor to 50 and 100 ppm acetone at 650 °C are measured and results obtained are shown in Figs. 11 and 12. It can be seen that, in Fig. 11**(a)**, the effect of RH on the responses of the sensor fabricated are small in the examined humidity range. As shown in Fig. 11**(b)**, The change amplitude of the response for fabricated sensor to 100 ppm acetone in the RH of 20%, 60% and 98% were 6.7%, −0.9% and −5.3%, which displayed little effect on the sensing performance of the sensor. Additionally, the stability of the sensor present fabricated was investigated by continuous working at high temperature of 650 °C during interval of 40 days. The responses of the sensor to 50 and 100 ppm acetone were measured every other day. And obtained results were recorded in Fig. 12. It can be seen that, from Fig. 12**(a)**, the change amplitude of the ΔV for the sensor attached with $NiNb_2O_6$-SE sintered at 1000 °C changed slightly to 50 and 100 ppm acetone during the 40 days measurement period.

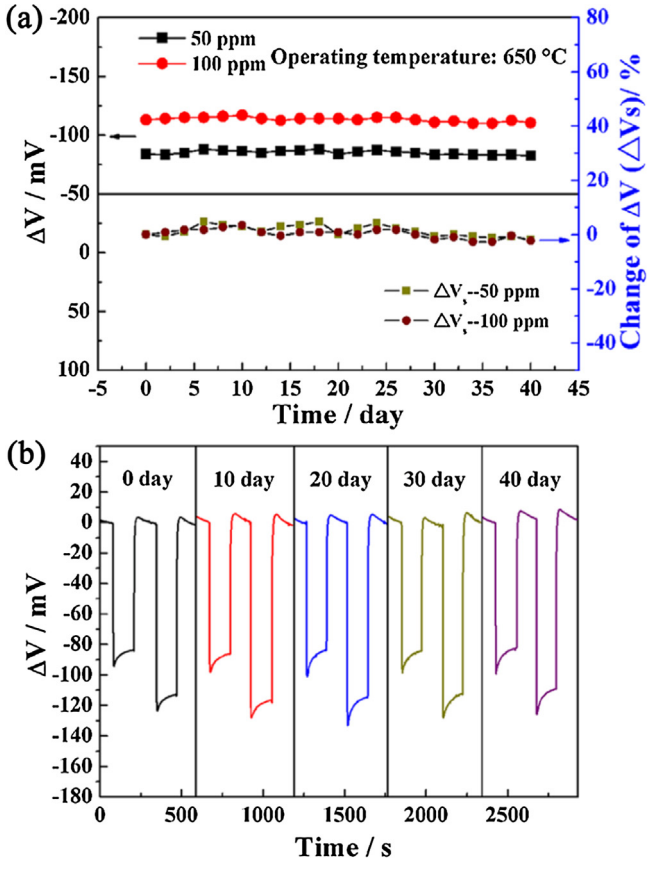

Fig. 12. (a) Long-term stability to 50 and 100 ppm acetone for the sensor attached with $NiNb_2O_6$-SE sintered at 1000 °C at 650 °C (b) response and recovery transients for the sensor using $NiNb_2O_6$-SE sintered at 1000 °C to 50 and 100 ppm acetone on the 0th, 10th, 20th, 30th and 40th days.

In order to further illustrate exactly the change amplitude of the ΔV with time, the change of the ΔV ($\triangle V_s$) for the sensor is given by $\triangle V_s = [(\Delta V_n - \Delta V_0)/\Delta V_0 \times 100\%]$, where ΔV_n and ΔV_0 denote the ΔV of the sensor on the n and 0 day, respectively. The quantitative results showed that the $\triangle V_s$ for the sensor to 50 and 100 ppm acetone on the 40th day were −1.8% and −2.2%, respectively. In order to better understand the changes in the process of aging, the response and recovery transients for the sensor using $NiNb_2O_6$-SE sintered at 1000 °C to 50 and 100 ppm acetone on the 0th, 10th, 20th, 30th and 40th days are shown in Fig. 12**(b)**. The result indicated that five response and recovery transients of the present device to 50 and 100 ppm acetone remain good consistency. Therefore, the present

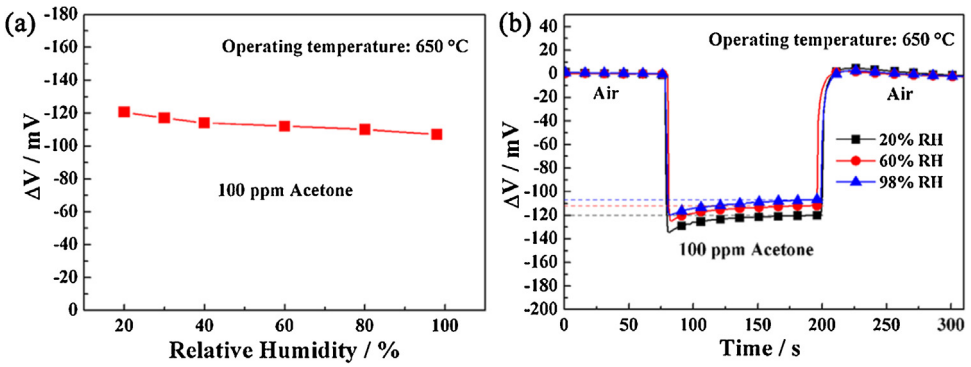

Fig. 11. (a) Response of the sensor attached with $NiNb_2O_6$-SE sintered at 1000 °C to 100 ppm acetone at 650 °C under different relative humidity (b) response and recovery transients for the sensor using $NiNb_2O_6$-SE sintered at 1000 °C to 100 ppm acetone under 20%, 60%, and 100% relative humidity at 650 °C.

Table 2
Comparison of the sensing performance of the present sensor and that of devices reported in literatures.

Material	Acetone Conc. (ppm)	Response (mV)	Sensitivity (mV/decade)	Humidity effect (98%)	Detection limit (ppm)	Reference
$NiNb_2O_6$	100	−113	−79	−5.3%	0.5	Present work
$Zn_3V_2O_8$	100	−69	−56	–	1	[18]
$NiCr_2O_4$	100	−60	−22	–	–	[16]
SnO_2	100	22	45	–	–	[17]
$Pt/CeO_2/SnO_2$	100	19	36	–	–	[17]
Porous $ZnO/ZnCo_2O_4$	100	7.5 ($R = R_a/R_g$)	–	–	10	[41]
Flower-like WO_3	100	17.4 ($R = R_a/R_g$)	–	–	1	[42]
Ce-doped SnO_2 hollow spheres	100	12 ($R = R_a/R_g$)	–	–	50	[43]
ZnO nanorod	100	30.4 ($R = R_a/R_g$)	–	–	1	[44]
$ZnFe_2O_4$ hollow microspheres	100	38 ($R = R_a/R_g$)	–	–	1	[45]
$ZnO/ZnFe_2O_4$ nanosheets	100	16.8 ($R = R_a/R_g$)	–	–	5	[46]

fabricated sensors also showed good water-vapor resistance and the excellent stability during the measurement period. Based on above results, the comparison of the acetone sensing property for the fabricated sensor and that reported previously in literature is presented in Table 2. Obviously, the present device exhibited better sensing performance to acetone than previously reported devices. The sensing performance of current sensor in sensitivity, low detection limit, water resistance and stability etc. showed that the sensor developed has a good application prospect in acetone detection.

4. Conclusion

The $NiNb_2O_6$ as a new sensing electrode material was synthesized via the facile sol–gel method and for the first time applied in construction of mixed potential type YSZ-based electrochemical gas sensors to detect acetone at 650 °C. The sensitivity of the sensor using $NiNb_2O_6$-SE annealed at different temperature was investigated and the result indicated that the sensor attached with $NiNb_2O_6$-SE sintered at 1000 °C displayed the largest sensitivity to acetone in the concentration range of 5–500 ppm, and that the present sensor showed the low detection limit of 500 ppb to acetone and excellent moisture resistance at 650 °C. In addition, the present device also exhibited good repeatability, acceptable selectivity and excellent stability in measurement period of 40 days at high-temperature-aging of 650 °C. For above-mentioned sensing performance of mixed potential type sensor fabricated, there is reason to believe that it can be considered as a potential candidate in the aspect of monitoring and diagnosing acetone.

Acknowledgments

This work is supported by Application and Basic Research of Jilin Province (20130102010JC), the National Nature Science Foundation of China (Nos. 61473132, 61134010, 61327804, 61374218 and 61377058), Program for Chang Jiang Scholars and Innovative Research Team in University (No. IRT13018) and National High-Tech Research and Development Program of China (863 Program, Nos. 2013AA030902 and 2014AA06A505).

References

[1] D. Dong, M. Shao, Y. Li, S. Lu, Y. Wang, Z. Ji, D. Tang, Carbonyl emissions from heavy-duty diesel vehicle exhaust in China and the contribution to ozone formation potential, J. Environ. Sci. 26 (2014) 122–128.
[2] J. Wang, L. Jin, J. Gao, J. Shi, Y. Zhao, S. Liu, T. Jin, Z. Bai, C. Wu, Investigation of speciated VOC in gasoline vehicular exhaust under ECE and EUDC test cycles, Sci. Total. Environ. 445–446 (2013) 110–116.
[3] G. Brown, A. Frankel, R. Hafner, Source apportionment of VOCs in the Los Angeles area using positive matrix factorization, Atmos. Environ. 41 (2007) 227–237.
[4] C. Cai, F. Geng, X. Tie, Q. Yu, J. An, Characteristics and source apportionment of VOCs measured in Shanghai, China, Atmos. Environ. 44 (2010) 5005–5014.
[5] J. Tsai, P. Huang, H. Chiang, Characteristics of volatile organic compounds from motorcycle exhaust emission during real-world driving, Atmos. Environ. 99 (2014) 215–226.
[6] M. Shnayderman, B. Mansfield, P. Yip, H. Clark, M. Krebs, S. Cohen, J. Zeskind, E. Ryan, H. Dorkin, M. Callahan, T. Stair, J. Gelfand, C. Gill, B. Hitt, C. Davis, Species-specific bacteria identification using differential mobility spectrometry and bioinformatics pattern recognition, Anal. Chem. 77 (2005) 5930–5937.
[7] S. Choi, W. Ryu, S. Kim, H. Cho, I. Kim, Bi-functional co-sensitization of graphene oxide sheets and Ir nanoparticles on p-type Co_3O_4 nanofibers for selective acetone detection, J. Mater. Chem. B 2 (2014) 7160–7167.
[8] L. Wang, A. Teleki, S. Pratsinis, P. Gouma, Ferroelectric WO_3 nanoparticles for acetone selective detection, Chem. Mater 20 (2008) 4794–4796.
[9] P. Sun, Y. Cai, S. Du, X. Xu, L. You, J. Ma, F. Liu, X. Liang, Y. Sun, G. Lu, Hierarchical α-Fe_2O_3/SnO_2 semiconductor composites: hydrothermal synthesis and gas sensing properties, Sens. Actuators B: Chem. 182 (2013) 336–343.
[10] X. Zhou, J. Liu, C. Wang, P. Sun, X. Hu, X. Li, K. Shimanoe, N. Yamazoe, G. Lu, Highly sensitive acetone gas sensor based on porous $ZnFe_2O_4$ nanospheres, Sens. Actuators B: Chem. 206 (2015) 577–583.
[11] J. Zosel, K. Ahlborn, R. Müller, D. Westphal, V. Vashook, U. Guth, Selectivity of HC-sensitive electrode materials for mixed potential gas sensors, Solid State Ionics 169 (2004) 115–119.
[12] L. Tang, Y. Li, K. Xu, X. Hou, Y. Lv, Selective acetone sensor based on its cataluminescence from nano-La_2O_3 surface, Sens. Actuators B: Chem. 132 (2008) 243–249.
[13] T. Nasution, I. Nainggolan, S. Hutagalung, K. Ahmad, Z. Ahmad, The sensing mechanism and detection of low concentration acetone using chitosan-based sensor, Sens. Actuators B: Chem. 177 (2013) 522–528.
[14] M. Mori, H. Nishimura, Y. Itagaki, Y. Sadaoka, Potentiometric VOC detection in air using 8YSZ-based oxygen sensor modified with $SmFeO_3$ catalytic layer, Sens. Actuators B: Chem. 142 (2009) 141–146.
[15] T. Xiao, X. Wang, Z. Zhao, L. Li, L. Zhang, H. Yao, J. Wang, Z. Li, Highly sensitive and selective acetone sensor based on C-doped WO_3 for potential diagnosis of diabetes mellitus, Sens. Actuators B: Chem. 199 (2014) 210–219.
[16] H. Zhang, C. Yin, Y. Guan, X. Cheng, X. Liang, G. Lu, NASICON-based acetone sensor using three-dimensional three-phase boundary and Cr-based spinel oxide sensing electrode, Solid State Ionics 262 (2014) 283–287.
[17] M. Kasalizadeh, A. Khodadadi, Y. Mortazavi, Coupled metal oxide-doped Pt/SnO_2 semiconductor and yittria-stabilized zirconia electrochemical sensors for detection of VOCs, J. Electrochem. Soc. 160 (2013) B218–B224.
[18] F. Liu, Y. Guan, R. Sun, X. Liang, P. Sun, F. Liu, G. Lu, Mixed potential type acetone sensor using stabilized zirconia and $M_3V_2O_8$ (M: Zn Co and Ni) sensing electrode, Sens. Actuators B: Chem. 221 (2015) 673–680.
[19] Q. Diao, C. Yin, Y. Guan, X. Liang, S. Wang, Y. Liu, Y. Hu, H. Chen, G. Lu, The effects of sintering temperature of $MnCr_2O_4$ nanocomposite on the NO_2 sensing property for YSZ-based potentiometric sensor, Sens. Actuators B: Chem. 177 (2013) 397–403.
[20] C. Wang, X. Cheng, X. Zhou, P. Sun, X. Hu, K. Shimanoe, G. Lu, N. Yamazoe, Hierarchical α-Fe_2O_3/NiO composites with a hollow structure for a gas sensor, ACS Appl. Mater. Interfaces 6 (2014) 12031–12037.
[21] H. Fan, Y. Zeng, H. Yang, X. Zheng, L. Liu, T. Zhang, Preparation and gas sensitive properties of ZnO–CuO nanocomposites, Acta Phys. Chem. Sin. 24 (2008) 1292–1296.
[22] P. Sun, X. Zhou, C. Wang, B. Wang, X. Xu, G. Lu, One-step synthesis and gas sensing properties of hierarchical Cd-doped SnO_2 nanostructures, Sens. Actuators B: Chem. 190 (2014) 32–39.
[23] G. Lu, N. Miura, N. Yamazoe, High-temperature sensors for NO and NO_2 based on stabilized zirconia and spinel-type oxide electrodes, J. Mater. Chem. 7 (1997) 1445–1449.
[24] N. Miura, J. Wang, M. Nakatou, P. Elumalai, S. Zhuiykov, M. Hasei, High-temperature operating characteristics of mixed-potential-type NO_2

sensor based on stabilized-zirconia tube and NiO sensing electrode, Sens. Actuators B: Chem. 114 (2006) 903–909.
[25] Q. Diao, C. Yin, Y. Liu, J. Li, X. Gong, X. Liang, S. Yang, H. Chen, G. Lu, Mixed-potential-type NO_2 sensor using stabilized zirconia and Cr_2O_3–WO_3 nanocomposites, Sens. Actuators B: Chem. 180 (2013) 90–95.
[26] V. Plashnitsa, T. Ueda, N. Miura, Improvement of NO_2 a sensing performances by an additional second component to the nano-structured NiO sensing electrode of a YSZ-based mixed-potential type sensor, Int. J. Appl. Ceram. Technol. 3 (2006) 127–133.
[27] N. Miura, T. Sato, S. Anggraini, H. Ikeda, S. Zhuiykov, A review of mixed-potential type zirconia-based gas sensors, Ionics 20 (2014) 901–925.
[28] Y. Su, X. Xin, Y. Wang, T. Wang, X. Wang, Unprecedented catalytic performance in disordered nickel niobate through photo-synergistic promotion, Chem. Commun. 50 (2014) 4200–4202.
[29] S. Lei, C. Wang, D. Guo, X. Gao, D. Cheng, J. Zhou, B. Cheng, Y. Xiao, Synthesis and magnetic properties of MNb_2O_6 (M = Fe, C. Ni) nanoparticles, RSC Adv. 4 (2014) 52740–52748.
[30] G. Lu, N. Miura, N. Yamazoe, High-temperature hydrogen sensor based on stabilized zirconia and a metal oxide electrode, Sens. Actuators B: Chem. 35–36 (1996) 130–135.
[31] N. Miura, H. Kurosawa, M. Hasei, G. Lu, N. Yamazoea, Stabilized zirconia-based sensor using oxide electrode for detection of NOx in high-temperature combustion-exhausts, Solid State Ionics 86–88 (1996) 1069–1073.
[32] N. Miura, G. Lu, N. Yamazoe, Progress in mixed-potential type devices based on solid electrolyte for sensing redox gases, Solid State Ionics 136–137 (2000) 533–542.
[33] P. Elumalai, J. Wang, S. Zhuiykov, D. Terada, M. Hasei, N. Miura, Sensing characteristics of YSZ-based mixed-potential-type planar NOx sensors using NiO sensing electrodes sintered at different temperatures, J. Electrochem. Soc. 152 (2005) H95–H101.
[34] G. Lu, Q. Diao, C. Yin, S. Yang, Y. Guan, X. Cheng, X. Liang, High performance mixed-potential type NOx sensor based on stabilized zirconia and oxide electrode, Solid State Ionics 262 (2014) 292–297.
[35] N. Miura, T. Raisen, G. Lu, N. Yamazoe, Highly selective CO sensor using stabilized zirconia and a couple of oxide electrodes, Sens. Actuators B: Chem. 47 (1998) 84–91.
[36] X. Liang, T. Zhong, H. Guan, F. Liu, G. Lu, B. Quan, Ammonia sensor based on NASICON and Cr_2O_3 electrode, Sens. Actuators B: Chem. 136 (2009) 479–483.
[37] N. Miura, M. Nakatou, S. Zhuiykov, Impedance-based total-NOx sensor using stabilized zirconia and $ZnCr_6O_4$ sensing electrode operating at high temperature, Electrochem. Commun. 4 (2002) 284–287.
[38] M. Stranzenbach, E. Gramckow, B. Saruhan, Planar, impedance-metric NOx-sensor with spinel-type SE for high temperature applications, Sens. Actuators B: Chem. 127 (2007) 224–230.
[39] H. Jin, Y. Huang, J. Jian, Sensing mechanism of the zirconia-based highly selective NO sensor by using a plate-like Cr_2O_3 sensing electrode, Sens. Actuators B: Chem. 219 (2015) 112–118.
[40] N. Miura, M. Nakatou, S. Zhuiykov, Impedancemetric gas sensor based on zirconia solid electrolyte and oxide sensing electrode for detecting total NOx at high temperature, Sens. Actuators B: Chem. 93 (2003) 221–228.
[41] X. Zhou, W. Feng, C. Wang, X. Hu, X. Li, P. Sun, K. Shimanoe, N. Yanazoe, G. Lu, Porous ZnO/$ZnCr_2O_4$ hollow spheres: synthesis, characterization, and applications in gas sensing, J. Mater. Chem. A. 2 (2014) 17683–17690.
[42] J. Huang, X. Xu, C. Gu, M. Yang, M. Yang, J. Liu, Large-scale synthesis of hydrated tungsten oxide 3D architectures by a simple chemical solution route and their gas-sensing properties, J. Mater. Chem. 21 (2011) 13283–13289.
[43] P. Song, Q. Wang, Z. Yang, Preparation, characterization and acetone sensing properties of Ce-doped SnO_2 hollow spheres, Sens. Actuators B: Chem. 173 (2012) 839–846.
[44] Y. Zeng, T. Zhang, M. Yuan, M. Kang, G. Lu, R. Wang, H. Fan, Y. He, H. Yang, Growth and selective acetone detection based on ZnO nanorod arrays, Sens. Actuators B: Chem. 143 (2009) 93–98.
[45] X. Zhou, X. Li, H. Sun, P. Sun, X. Liang, F. Liu, X. Hu, G. Lu, Nanosheet-assembled $ZnFe_2O_4$ hollow microspheres for high-sensitive acetone sensor, ACS Appl. Mater. Interfaces 7 (2015) 15414–15421.
[46] X. Li, C. Wang, H. Guo, P. Sun, F. Liu, X. Liang, G. Lu, Double-shell architectures of $ZnFe_2O_4$ nanosheets on ZnO hollow spheres for high- performance gas sensors, ACS Appl. Mater. Interfaces 7 (2015) 17811–17818.

Biographies

Fangmeng Liu received his B.S. degree in 2009 from College of Chemistry, Liaocheng University and M.S. degree in 2012 from Northeast Forestry University in China. Currently he is studying for his Ph.D. degree in College of Electronic Science and Engineering, Jilin University, China.

Xue Yang received the B.Eng. degree in department of electronic science and technology in 2015. She is currently studying for his M.E. Sci. degree in College of Electronic Science and Engineering, Jilin University, China.

Bin Wang received the B.Eng. degree in department of electronic science and technology in 2015. He is currently studying for his M.E. Sci. degree in College of Electronic Science and Engineering, Jilin University, China.

Yehui Guan received the B.Eng. degree in department of electronic science and technology in 2014. He is currently studying for his M.E. Sci. degree in College of Electronic Science and Engineering, Jilin University, China.

Xishuang Liang received the B. Eng. degree in Department of Electronic Science and Technology in 2004. He received his Doctor's degree in College of Electronic Science and Engineering at Jilin University in 2009. Now he is an associate professor of Jilin University, China. His current research is solid electrolyte gas sensor.

Peng Sun received his PhD degree from the Electronics Science and Engineering department, Jilin University, China in 2014. Now, he is engaged in the synthesis and characterization of the semiconducting functional materials and gas sensors.

Geyu Lu received the B.Sci. degree in electronic sciences in 1985 and the M.S. degree in 1988 from Jilin University in China and the Dr. Eng. degree in 1998 from Kyushu University in Japan. Now he is a professor of Jilin University, China. His current research interests include the development of chemical sensors and the application of the function materials.